PREPRINT SUBMITTED

tektonika

A semi-automated method for constructing three-dimensional models of complex fault networks

A. Howell[1,2]*, T. McLennan[3], C. Penney[1], A. Nicol[1], H. Seebeck[2], R. Van Dissen[2], C. Williams[2] & B. Fry[2]

[1]School of Earth and Environment, Te Whare Wānanga o Waitaha — University of Canterbury, Aotearoa New Zealand
[2]Te Pū Ao — GNS Science, Lower Hutt, Aotearoa New Zealand
[3]Seequent, The Bentley Subsurface Company, Christchurch, Aotearoa New Zealand
**Corresponding author (e-mail: a.howell@gns.cri.nz)*

Abstract

Fault geometry and the connectivity between faults at depth are both important controls on the nucleation, propagation and arrest of earthquake rupture, so modelling these parameters accurately is essential to models of the earthquake cycle. However, simulations involving complex three-dimensional (3D) fault systems rarely explore the sensitivity of results to uncertainties in geometry and connectivity — either in terms of modelled earthquake characteristics or impacts such as ground shaking and surface deformation. In many cases, geometry-related sensitivity testing is limited because it is challenging to construct a suite of alternative fault models that span the range of plausible fault geometries, intersections and connections; such alternative models are especially difficult to construct for systems where faults truncate or cross-cut each other at depth. We present a new, semi-automated method that simplifies creation of 3D models of networks of tens or hundreds of faults, combining open-source python tools with the meshing capabilities of Leapfrog™ software. The new workflow reduces the time to create a fault model of 113 faults in central Aotearoa New Zealand by ∼80%, from 25 hours to 5 hours of human input. This improvement significantly decreases the effort required to create multiple alternative fault geometries, making detailed sensitivity analyses more feasible. The applicability of the workflow is demonstrated for the creation of three alternative models of fault geometries for central Aotearoa New Zealand.

1 Introduction

Three-dimensional (3D) models of fault networks have many important applications in the earth sciences. For example, in earthquake science, 3D representations of active faults underpin seismic hazard models (e.g., Field et al., 2014; Pagani et al., 2020; Gerstenberger et al., 2020); next-generation tsunami hazard models (Hughes et al., 2023); earthquake slip inversions (e.g., Hamling et al., 2017; Elliott et al., 2012; Liu et al., 2019); and dynamic and kinematic models of earthquake rupture processes (e.g., Lozos, 2016; Ando and Kaneko, 2018; Ulrich et al., 2019a; Shaw et al., 2022). These applications generally include pre-defined fault surface geometries, which may influence model outputs, including ground shaking and tsunami hazard (Satake et al., 2022). The structural complexity of fault systems is well established, and has become even better defined as more subsurface data have been made available. Meanwhile, high-resolution observations of earthquake deformation and more complex physics-based models of earthquake behaviour have demonstrated that fault geometry is a key control on earthquake behaviour across multiple temporal and spatial scales (Howarth et al., 2021; Mildon et al., 2019; Delogkos et al., 2023; Oglesby and Mai, 2012). It is therefore essential to incorporate realistic fault geometries in both numerical models of the earthquake cycle and also seismic and tsunami hazard models (e.g., Faure Walker et al., 2018; Satake et al., 2022). Despite its importance, there are often significant uncertainties in subsurface geometry — especially surrounding the dip angle of faults at depth and the ways that some faults terminate against or intersect other faults (Seebeck et al., 2023). It is sometimes possible to assess the sensitivity of model results to uncertainties in these parameters through the creation of multiple alternative fault geometries (Ando and Kaneko, 2018; Hamling et al., 2017; Delogkos et al., 2023; Mildon et al., 2019). However, in practice the large amount of time and effort required to model alternative fault geometries often limits the scope of sensitivity analyses (Delogkos et al., 2023).

In this study, we present a workflow for the rapid creation of triangular mesh surfaces representing complex fault systems, demonstrating the workflow's utility by creating several alternative models of a complex system of faults in the north-eastern South Island of Aotearoa New Zealand. This workflow uses a combination of new, open-source python tools together with the meshing and mesh-cutting capabilities of proprietary Leapfrog Geo software. The python tools and documentation are available from https://github.com/uc-eqgeo/cfm_leapfrog.

2 Previous approaches to fault model construction

Many 3D models of complex fault systems have been created globally. Notable examples of 3D models covering regions that are hundreds or thousands of kilometres wide include the Southern California Earthquake Centre (SCEC) Community Fault Model (Plesch et al., 2007, 2020) and fault models from Japan (Fujiwara et al., 2009), Taiwan (Chan et al., 2020), Greece (Caputo et al., 2012), Malawi (Williams et al., 2022), Aotearoa New Zealand (Seebeck et al., 2022, 2023) amongst other areas. In general, these large-scale fault models were created using one of two approaches (summarised by Seebeck et al., 2023):

1. Generation of 3D fault polygons through projection of fault surface traces to depth using a constant average dip and specified dip azimuth. Major advantages of this approach are that it is easy to implement automatically and sufficiently accurate for most Probabilistic Seismic Hazard Assessment (PSHA) applications. The main disadvantage of the approach is that changes in strike between adjacent segments of the same fault can lead to the creation of either gaps where a fault surface should be present or regions where two parts of a fault intersect and even pass through each other. These gaps and intersections can impact model outputs, especially for physics-based models that rely on modelling stress interactions between fault sections or elements to simulate earthquake rupture.

2. Generation of complex fault meshes using dedicated geological modelling software packages like SKUA-GOCAD™ or MOVE™. This approach allows the creation of detailed fault surfaces with smooth transitions between segments of different strike, as well as trimming of fault surfaces so that some faults terminate against others without passing through them. Approach 2 is preferable to the simpler method above for applications that require more detailed representations of fault surfaces, but requires significantly manual effort — often weeks or months for a complex network of hundreds of faults. Furthermore, following this approach it is laborious to create alternative models of fault geometry for a complex fault network, (e.g. to test sensitivity of simulation results to fault geometry). Despite its time consuming nature, this type of approach remains the preferred approach to create an accurate geometric representation of a large fault network; example of its use include the

California Community Fault Model (Plesch et al., 2007) and the Aotearoa New Zealand Community Fault Model (NZ CFM hereafter; Seebeck et al., 2023).

In addition to these two broad categories of methods for fault model construction, there are several software workflows available for the automatic or semi-automatic construction of 3D models of fault networks. Examples include: the meshing workflow for SeisSol (https://github.com/SeisSol/Meshing), which has been used to create models of complex fault networks for use simulations of dynamic rupture in recent earthquakes (e.g. Ulrich et al., 2019a,b); and the 3D-Faults code of Mildon et al. (2016), available at https://github.com/ZoeMildon/3D-faults. Other codes exist that are not yet publicly available; one such code was used to create a fault model of New Zealand by Shaw et al. (2022), but produces less realistic fault surfaces than the manual approach used for the NZ CFM by Seebeck et al. (2022, 2023). However, we are unaware of any automated or semi-automated workflow that has been used to create detailed representations of fault surfaces in a network of hundreds of faults. The semi-automated method we present here is intended to allow the creation of a 3D model of hundreds of faults with the minimum of manual effort, and to support time-efficient generation of alternative models for sensitivity analyses.

2.1 The Aotearoa New Zealand Community Fault Model

The NZ CFM (v1.0) comprises simplified representations of 880 faults or fault segments across the New Zealand plate boundary zone (684,000 km^2) for which late Quaternary slip has been established or was deemed possible (Seebeck et al., 2022, 2023). The NZ CFM provides the basis for applications such as the New Zealand National Seismic Hazard Model's (NZ NSHM 2022) geologic and geodetic deformation models (Gerstenberger et al., 2024a,b; Johnson et al., 2024; Van Dissen et al., 2024) through the geometric and kinematic description of faults with the potential to generate damaging earthquakes generally greater than M_W 6. This simplified model of upper crustal faulting encompasses a wide spectrum of fault types, dominated by gently to steeply dipping upper-crustal faults that intersect the ground surface, and large variably-dipping subduction interfaces. The NZ CFM provides a more comprehensive fault characterisation for the New Zealand plate boundary than previous regional fault models (Stirling et al., 2012; Litchfield et al., 2014).

Each fault in the NZ CFM is represented as a GIS line approximating surface or seafloor traces (or the surface projection of the fault in the case of blind faults), with an attached structured table of fault parameter attributes. These fault parameters define the geometry of each fault or fault segment along with kinematic parameters quantifying sense of movement and slip rate, the details of which are provided in Seebeck et al. (2022, 2023). The use of the term "segment" is consistent with previous New Zealand fault models (e.g., Litchfield et al., 2014) and defines dip, rake and/or slip rate changes along-strike between segments. Fault segmentation in the NZ CFM is solely a geometric and kinematic description and is not intended to convey information about the location of earthquake rupture segments (e.g., Wesnousky, 2008). The initial 3D fault geometries were built with MOVE^{TM} geological modelling software using the GIS-referenced fault traces as initial constraints with all crustal faults projected down-dip from mean sea-level (0 m elevation) perpendicular to their average strike using the 'preferred' dip estimate (e.g., Plesch et al., 2007) to a maximum depth of fault rupture. Projection of faults from mean sea-level is a requirement of downstream applications such as the NZ NSHM 2022 (Gerstenberger et al., 2024a,b) and physics-based earthquake simulators like RSQSim (Richards-Dinger and Dieterich, 2012). Two down-dip depths are provided in the NZ CFM: a seismically determined limit of faulting (D90); and a maximum fault rupture depth derived from a combination of D90 and thermal-fault friction models that includes an extra factor representing rupture propagation into the conditional stability zone (Ellis et al., 2024). The initial 3D fault geometries developed for the NZ CFM predominantly use the maximum depth of fault rupture or intersection with major structures, such as subduction thrusts, to constrain the down-dip fault dimension.

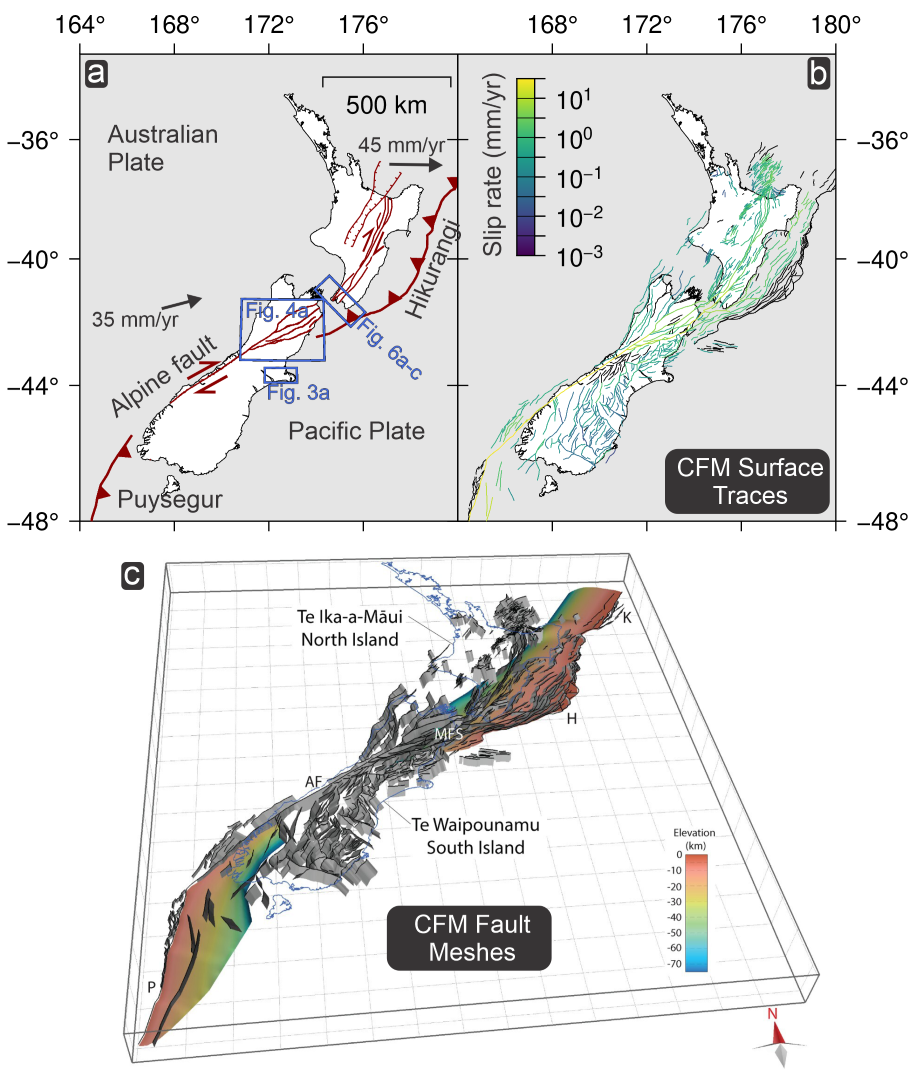

Figure 1: The Aotearoa New Zealand Community Fault Model (NZ CFM). (a) Tectonic setting of Aotearoa New Zealand, showing the Hikurangi and Puysegur subduction zones, schematic representations of major crustal fault systems and indicative rates and directions of Australia-Pacific Plate motions (Beavan et al., 2002). Boxes show regions of interest for the Greendale Fault (Figure 3a) and Hope Fault (Figure 4a) and the coastal Wellington Region (Figure 6a-c). (b) Traces of crustal faults in the NZ Community Fault Model (Seebeck et al., 2023), coloured by preferred slip rate. Faults with no assigned slip rate in the model are shown in black. (c) 3D perspective representation of the NZ CFM, created using MOVE™ software. P, H and K are the Puysegur, Hikurangi and Kermadec subduction zones. AF is the Alpine Fault and MFS is the Marlborough Fault System.

3 Fault Construction Workflow

There are several steps to our workflow for fault surface creation, which can be summarized as follows (and also in Figure 2):

1. Generate depth contours for creation of fault surfaces using surface traces and average dip information.
2. Modify depth contours for connected (multi-segment) faults.
3. Build triangular meshes representing each fault geometry using the fault traces and depth contours.
4. Trim the fault meshes, either to the area where contours have been generated, or against other faults.

To simplify the explanation of our workflow, we describe it by focussing on two example faults from the South Island of Aotearoa New Zealand. The first example is the Greendale Fault (Figure 3), the only fault that ruptured the ground surface in the M_W 7.1 Darfield earthquake in 2010. This fault is isolated from other nearby major faults, which makes it a good example to demonstrate our treatment of a "simple" (single-segment) fault — although we note that the NZ CFM representation is a significant simplification of several smaller faults that ruptured together in 2010 (Villamor et al., 2012; Elliott et al., 2012; Beavan et al., 2012). Our second example is the Hope Fault (Figure 4), which is more complicated to model: it is formed of seven different segments, with subtly different strikes and dips, the western-most of which terminates against the Alpine Fault.

The primary input for our workflow is a GIS representation of fault traces, with dip and dip direction attached as metadata (Step 1 in Figure 2). For the our Aotearoa New Zealand example, these data were compiled in a series of community workshops and form a major part of the NZ CFM (Seebeck et al., 2022, 2023). We also use slip-rate metadata (another product of the NZ CFM community workshops) to inform which faults terminate against other faults, although these terminations can also be specified without providing slip-rate data.

3.1 Defining multi-segment faults

Many faults in the New Zealand network can be thought of as isolated single-segment faults (our Greendale example), but often it is necessary to join fault segments together into a larger "connected", multi-segment fault (such as our Hope Fault example). In the python pre-processing part of our workflow, we identify fault segments that may be connected to each other on the basis of horizontal distance between fault traces. If the minimum distance between the end points of two traces is less than a threshold (200 m for our central Aotearoa New Zealand model), we assign the two fault segments as possible neighbouring segments in a connected multi-segment fault. We use the networkx library (Hagberg et al., 2008) in python to create a network of fault segments that connect with each other (Step 2 in Figure 2) and write the names of the segment in each connected set of segments to a text file, which we edit manually (Step 3 in Figure 2).

Manual editing is necessary because the traces of many of the fastest-slipping faults — for example, the Alpine, Hope, Wairau, Awatere and Jordan–Kekerengu–Needles faults — form one large connected network (shown without fault names in Figure 4a), which needs to be separated into its constituent faults before they can be modelled. It might be possible to perform this separation automatically based on patterns in the names of fault segments, but we prefer to define the segments that make up multi-segment faults manually for two reasons. First, the manual editing step means that we do not rely on a naming convention specific to this data set. Second, fault segments have often been named based on surface geological mapping, but in some cases it makes more geometric sense to connect faults in a way that is inconsistent with naming conventions. For example, for our Hope Fault example (Figure 4b), we chose to include the Kelly Fault as a segment of the (multi-segment) Hope Fault due to its high slip rate and along-strike continuity with the other segments. This somewhat subjective choice means that the "Hope: Taramakau" is modelled as a separate fault that terminates against the multi-segment fault; this specification of possible subsurface geometry would not be possible if our method relied on naming conventions.

3.2 Cutting hierarchy of faults

Before the fault system is meshed in Leapfrog, it is necessary to prescribe which faults (or fault systems) will cut other faults, and which faults will terminate against others. We specify a cutting hierarchy, which is simply an ordered list of fault names. If two fault surfaces intersect, the fault that is lower in the cutting hierarchy (appears later in the list) is cut by the fault that is higher in the hierarchy (appears earlier in the list).

In general in Aotearoa New Zealand, we assume that slower-slipping faults terminate against faster-

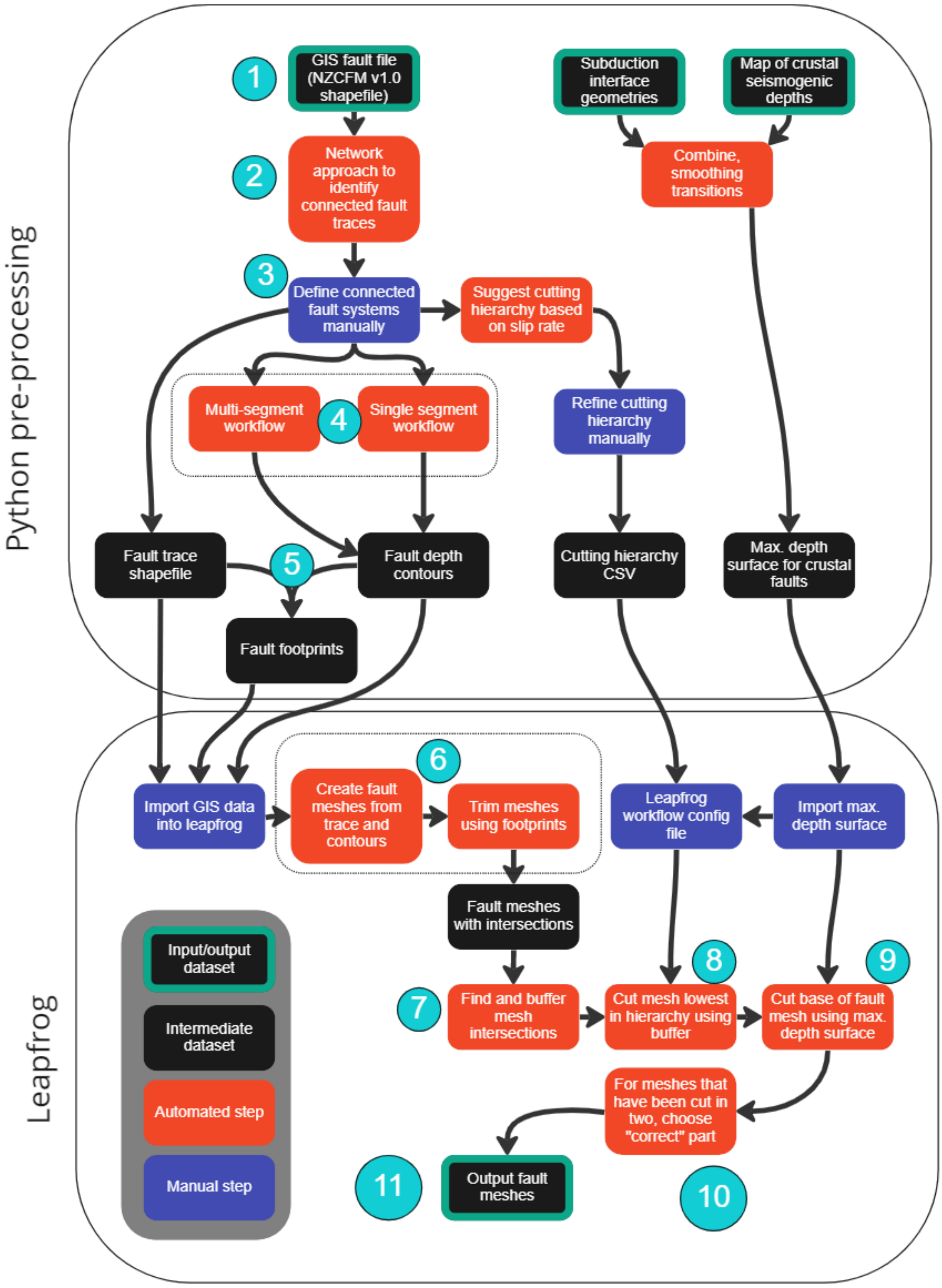

Figure 2: Workflow for the creation of meshed fault surfaces using our methodology. Numbers represent major steps in the workflow that are referenced in the text.

slipping faults (after Robinson, 2004; Robinson et al., 2011), so that we can generate a reasonable first-pass hierarchy by sorting faults or fault systems in descending order of slip rate. For connected fault systems where different segments have different slip rates, we use the maximum slip rate to determine the position of the fault system in the cutting hierarchy. We write this hierarchy to a text file and edit manually to account for a few exceptions to this rule. The Jordan–Kekerengu–Needles Fault is an example of such an exception; it has a maximum preferred NZ CFM slip rate of 23 mm/yr (Seebeck et al., 2023), yet is thought to terminate against the Hope Fault (maximum preferred slip rate 17.3 mm/yr). Consequently, the Jordan–Kekerengu–Needles Fault is moved below the Hope fault system in the the cutting hierarchy. The cutting hierarchy for our example fault network can be found in the supplementary data (Howell et al., 2025).

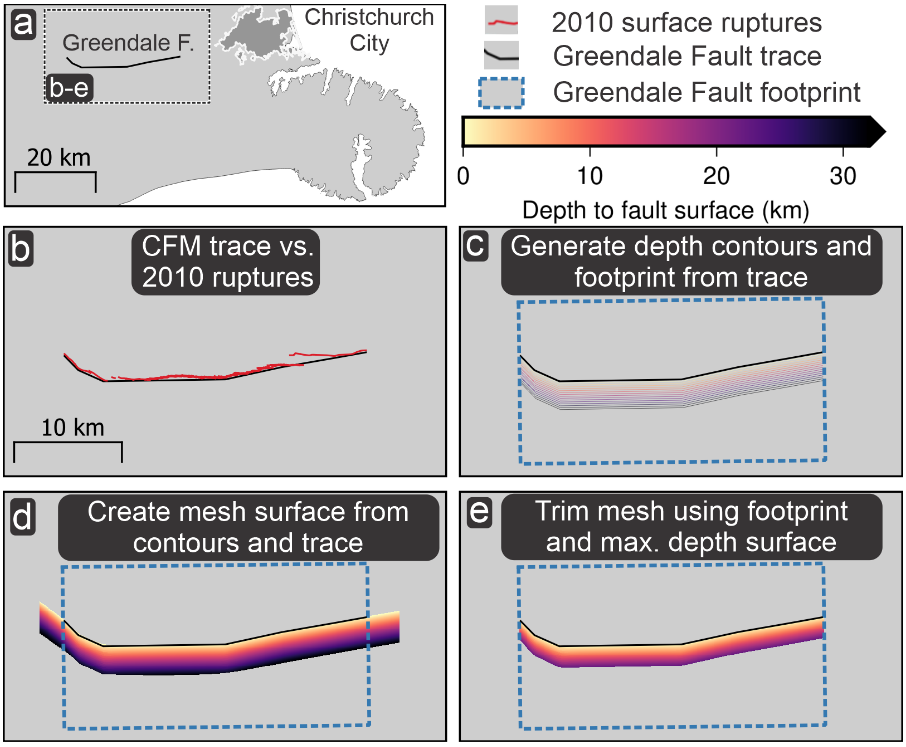

Figure 3: Illustration of our workflow applied to the Greendale Fault in central Aotearoa New Zealand. (a) Location of the Greendale Fault relative to nearby Christchurch. (b) Mapped surface ruptures from the 2020 Darfield earthquake (red; Villamor et al., 2012) and the NZ CFM approximation of the surface trace. (c) Depth contours created by extrapolating from the surface trace and a constant dip, and fault footprint (Step 5 in Figure 2). (d) 3D triangular mesh generated from contours and surface trace using Leapfrog's radial basis function (RBF) meshing algorithm. (e) Final mesh, after trimming using the fault footprint and the smoothed maximum depth surface (Steps 6 and 9 in Figure 2).

3.3 *Creation and clipping of depth contours*

Our workflow uses python pre-processing to create depth contours for faults by projecting surface traces down dip (Figures 3 and 4. The contours — created at 2 km depth intervals in this study — are then read into Leapfrog and meshed into surfaces. For single-segment faults like the Greendale Fault, the creation of contours is simple; contours are created by translating the surface trace to depth assuming a constant dip and dip direction (dip direction is perpendicular to average strike; Figure 3). For the more complex multi-segment faults like the Hope Fault, we shorten contours at depth where there are changes in strike or dip between adjacent segments of the fault (Figure 4). Shortening these contours serves two important purposes. First, the shortening prevents contours from neighbouring segments from intersecting or crossing each other, which could cause meshed fault surfaces to have unrealistic geometries. Second, the shortening of contours allows the user to constrain the smoothness of transitions between neighbouring segments of a fault in a consistent way.

The amount by which contours are shortened at depth is subjective and depends on user preference; it is governed by the equation:

$$\Delta L = \frac{\alpha_{trim} \cdot Z \cdot tan(\Theta_{change})}{sin(\delta_{dip})} \tag{1}$$

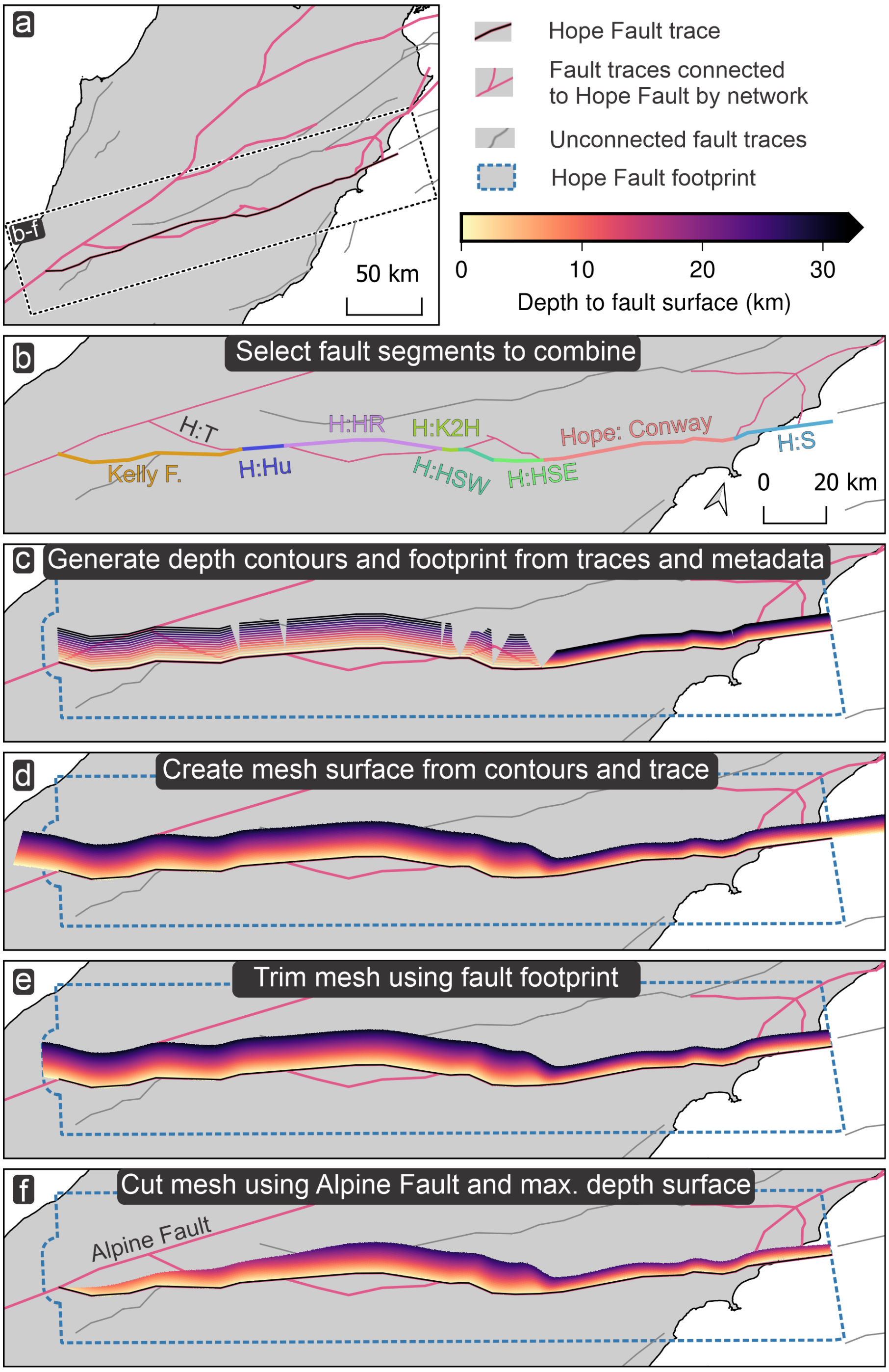

Figure 4: Illustration of our workflow applied to the Hope Fault in central Aotearoa New Zealand. (a) Hope Fault trace (black) and other fault segments assigned to the same fault network by our networkx filter (pink). Other (unconnected) fault segment traces are coloured grey. (b) Segment traces and names for our multi-segment Hope Fault model. H:T is Hope: Taramakau; H:Hu is Hope: Hurunui; H:HR is Hope: Hope River; H:K2H is Hope: Kakapo to Hanmer; H:HSW is Hope: Hanmer SW; H:HSE is Hope: Hanmer SE; H:S is Hope: Seaward. Note that the Kelly Fault is included as part of our multi-segment Hope Fault model, but Hope: Taramakau is not. (c) Depth contours generated by projected segment surface traces down dip and trimming them near segment boundaries. The multi-segment fault footprint is marked by a blue dashed line. (d) Mesh created by interpolation between contours in Leapfrog. (e) Mesh trimmed using fault footprint. (f) Final mesh, trimmed using the maximum depth surface (Ellis et al., 2024) as well as the Alpine Fault at the western end.

In Equation 1, ΔL is the length that is trimmed from one end of a depth contour. α_{trim} is a constant, dimensionless "trimming factor" that can be adjusted for linear scaling of ΔL; for our central Aotearoa New Zealand example, we set α_{trim} to 1. Z is the depth of the contour in the same units as ΔL, and δ_{dip} is the average dip of the segment of the fault system. Θ_{change} is an angle that we use to represent the difference in either average strike or dip between the fault segment and its immediate neighbour. The choice of Θ_{change} is subjective, but based on trial and error, we set it to either the difference in segment dip, or half the difference in strike, whichever is greater. We only trim contours at the junctions between adjacent segments of a fault system; contours of the two end segments of a connected fault system — which each have only one neighbour — are only cut at one end (Figure 4).

3.4 Fault footprints

When a mesh is created from contours or other data using Leapfrog software, the edges of the mesh are defined by a 3D bounding box. By default, the edges of a bounding box are parallel to the axes of a standard Cartesian coordinate system: the east, north and up directions. However, for the purposes of our fault model, the edges of most of our meshed fault surfaces should run perpendicular to the strike of the surface trace. We therefore create fault "footprints" to replace the standard Leapfrog bounding boxes and control the edges of our fault surfaces (Step 5 in Figure 2). These footprints are created by calculating a horizontal buffer (10 km for all the faults discussed here) around the the fault trace and depth contours together, and modifying this buffer depending on characteristics of the fault of interest. Examples of footprints are shown for the Greendale (Figure 3) and Hope faults (Figure 4). For a single-segment fault that does not connect with any other faults in the network, the footprint is cut so that it forms an edge running perpendicular to the overall strike of the fault segment (Figure 3). For any end of a connected fault system that does not terminate against another fault, the edge of the footprint runs perpendicular to the average strike of the end-most segment of the fault system (for example, the eastern end of the Hope Fault; Figure 4).

For faults that terminate against other faults, it is necessary to allow for the faults to dip in opposite directions without leaving a gap at depth where the meshed surfaces should intersect. Therefore, where a fault is expected to be cut by another fault, we add a buffer to the edge footprint to allow the meshed surface to extend beyond the fault trace and contours. An example of such a treatment is the western end of the Hope Fault (Figure 4). At this western end, the Hope Fault will be cut by the Alpine Fault, so that the footprint edge does not need to constrain the edge of the meshed fault surface.

3.5 Seismogenic depths

Like many tectonically-active regions worldwide, Aotearoa New Zealand has significant spatial variations in seismogenic depth, from $\sim$8km in the Taupō Volcanic Zone to $>$ 25 km in the southern South Island (Ellis et al., 2021, 2024). For a model of active crustal faults, it is important to incorporate these variations in seismogenic depth as well as the fact that many faults are truncated at depth by either the Hikurangi (Williams et al., 2013) or Puysegur subduction zones (Seebeck et al., 2022, 2023). We incorporate these changes in seismogenic depth by using or creating surfaces to represent maximum seismogenic depths throughout Aotearoa New Zealand. We calculate depth contours to 32 km depth and then use these seismogenic depth surfaces to truncate the base of the meshed fault surfaces. To avoid sudden along-strike steps in the base of fault surfaces, we smooth the depth surface of Ellis et al. (2024) using a 50 km-wide moving mean before trimming fault surfaces.

3.6 Meshing and trimming fault surfaces using Leapfrog software

The Leapfrog component of our workflow takes five inputs, the creation of which we have described in Sections 3.1 to 3.5: fault surface traces, depth contours and footprints, as well as a text file defining the cutting hierarchy and 2D grid of elevations representing seismogenic depths. After reading in these input data, the depth contours are used to create fault mesh surfaces formed of triangular elements, with any gaps between contours filled by radial basis function (RBF) interpolation (Step 6 in Figure 2). The lateral extent of these meshed fault surfaces is then trimmed using the footprints and the base seismogenic depth surface (Steps 6 and 9; Figure 2) described in Section 3.4.

For faults that intersect other faults, we use Leapfrog to identify intersections between meshed fault surfaces automatically (Step 7 in Figure 2). We create buffer surfaces around these intersections: each intersection is a 3D line and the buffer is a 3D isosurface at a constant distance from the intersection line (Step 8; Figure 2). The purpose of the buffers is to eliminate intersections between different faults, since these intersections can cause stress singularities when fault models are used for some specific downstream applications, such as physics-based earthquake simulators (e.g. Shaw et al., 2022). For the example in this paper, we use a buffer size of 1 km, although this value should be changed based on the intended application of the fault meshes; it should be sufficiently large that intersections are not re-introduced if fault surfaces are later re-meshed. If the intersection is only partial, the buffer region is simply removed from the fault surface, leaving a slot along the intersection line. If the intersection extends across the whole fault surface, i.e. bisects the surface, our workflow determines which section of the fault to keep based on proximity to the fault surface trace (step 10 in Figure 2).

4 Application

The focus of this study is primarily methodological, being the creation of a new, time-efficient workflow for fault model creation. However, to demonstrate the utility of the workflow, we present: (1) a 3D fault model for central Aotearoa New Zealand developed using the workflow; and (2) three alternative possible geometric models for major faults that cross the coast in the Greater Wellington Region.

4.1 Fault model for central Aotearoa New Zealand

An oblique view of a model of 113 faults in central Aotearoa New Zealand is shown in Figure 5; it took 5 hours to create and is included here to demonstrate a successful application of our workflow. This model is based on the same inputs as the NZ CFM, but its creation using our workflow allowed us to adjust two aspects of the model to improve its suitability for one intended use case, generation of a synthetic earthquake catalogue using the RSQSim earthquake simulator (Richards-Dinger and Dieterich, 2012). First, our workflow adds small gaps (buffers) at locations where two fault surfaces would otherwise intersect, which avoids stress singularities in RSQSim. Second, our fault model uses a smoothed version of the maximum rupture depth surface of Ellis et al. (2021, 2024), which allows us to improve the way slip rate tapers towards the base of fault surfaces in RSQSim. In contrast, crustal faults in the NZ CFM that are not located near a subduction interface terminate at a constant depth. Our approach allows a long fault to have significant variations in seismogenic depth along its length.

4.2 Alternative models of fault geometry for coastal areas of the Greater Wellington Region

A second example of an application of our workflow is the creation of alternative (plausible) fault models for the modelling of coseismic coastal deformation hazard, using the case study of the Greater Wellington Region in central Aotearoa New Zealand. Over the course of Aotearoa New Zealand's short (∼180 year) historical record, several earthquakes have caused significant uplift and subsidence of its coastline with significant impacts on coastal communities; examples include the AD 1855 Wairarapa, 1931 Napier, 1987 Edgecumbe, 2011 Christchurch and 2016 Kaikōura earthquakes (Darby and Beanland, 1992; Hull, 1990; Hughes et al., 2015; Clark et al., 2017; Delano et al., 2022). From a coastal hazards perspective, it is therefore important to understand possible deformation in future coastal earthquakes (Naish et al., 2024). However, although the sensitivity of coseismic vertical coastal motions to fault geometry is well understood (Okada, 1985; Delano et al., 2023), the dips of many coastal faults remain poorly constrained.

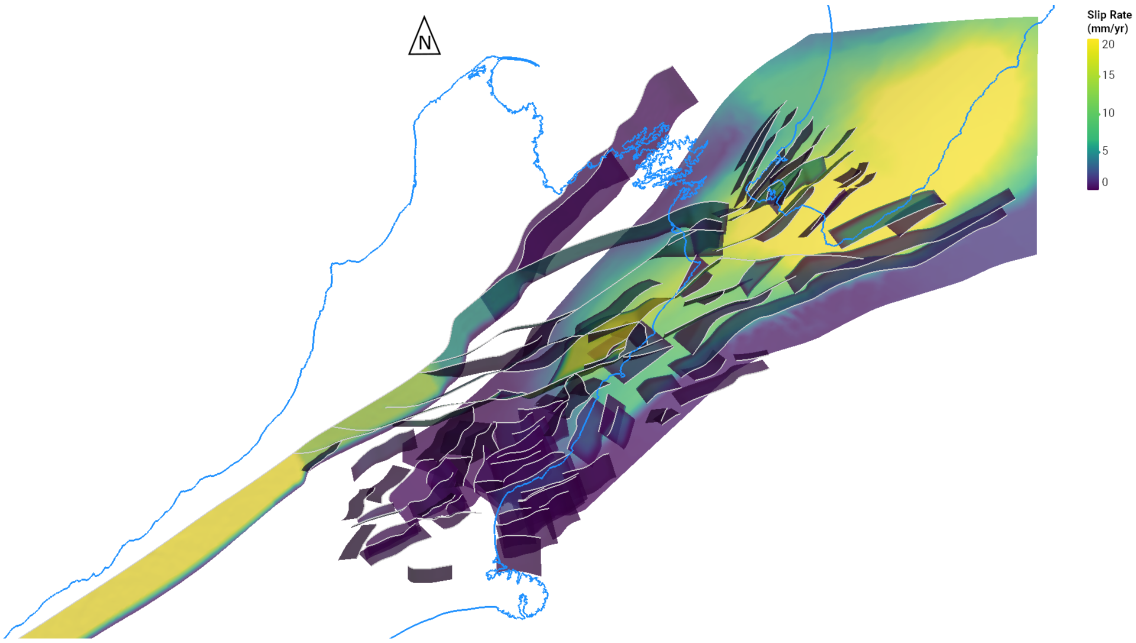

Figure 5: A 3D representation of a fault network model for central Aotearoa New Zealand created using our workflow. Slip rates are based on those of Van Dissen et al. (2024), but crustal fault slip rates taper to zero close to fault edges and the base of faults. The Hikurangi subduction interface surface shown here (truncated at 40 km depth) not created as part of our workflow; it is from (Williams et al., 2013) and is used to truncate the base of some crustal fault meshes.

To gauge uncertainties in coseismic vertical displacement hazard (Delano et al., 2024), it is necessary to model several alternative — but plausible — fault geometries.

Cross sections through three different model geometries of coastal faults in the Greater Wellington Region are shown in Figure 6. The two alternative models (Figures 6c-d) to the NZ CFM geometry (Figure 6b) were developed with input from local experts and both represent plausible (simplified) configurations of faults in the area of interest. Without a workflow like the one proposed here, it would be labour intensive to create a suite of 3D models of the fault networks, mainly because changing the dips of multiple faults simultaneously alters the depths at which some faults terminate against each other or the Hikurangi subduction interface. However, using our workflow it was possible to create the three alternative 3D fault models in $\sim$4 hours. The differences between modelled coseismic coastal vertical displacement hazard between the three models presented here demonstrate the importance of considering sensitivity to fault geometry — changing the probability of exceeding 0.2 m coseismic subsidence in the next 100 years by a factor of 3 (5% to 15%) at some sites. For more details, refer to Delano et al. (2024).

5 Limitations and possible future work

The workflow presented above represents a relatively efficient way to generate a 3D model of a network of hundreds of faults, compared with the more manual workflow employed to build v1.0 of the NZ CFM. However, the workflow remains a work in progress, and we now list several ways that future work could improve it.

Complex fault intersections at depth. In most regional- or national-scale fault networks likely to be modelled using our workflow, there will be intersections in the subsurface between modelled fault surfaces. Our workflow features many areas where two fault surfaces project past each other at depth, resulting in a conjugate cross-cutting geometry. Such cross-cutting fault structures may be realistic in some locations, but for some faults (e.g., antithetic faults) it may be more realistic to avoid this by ensuring that faults terminate at shallower depths, or specifying a "master" fault. Future im-

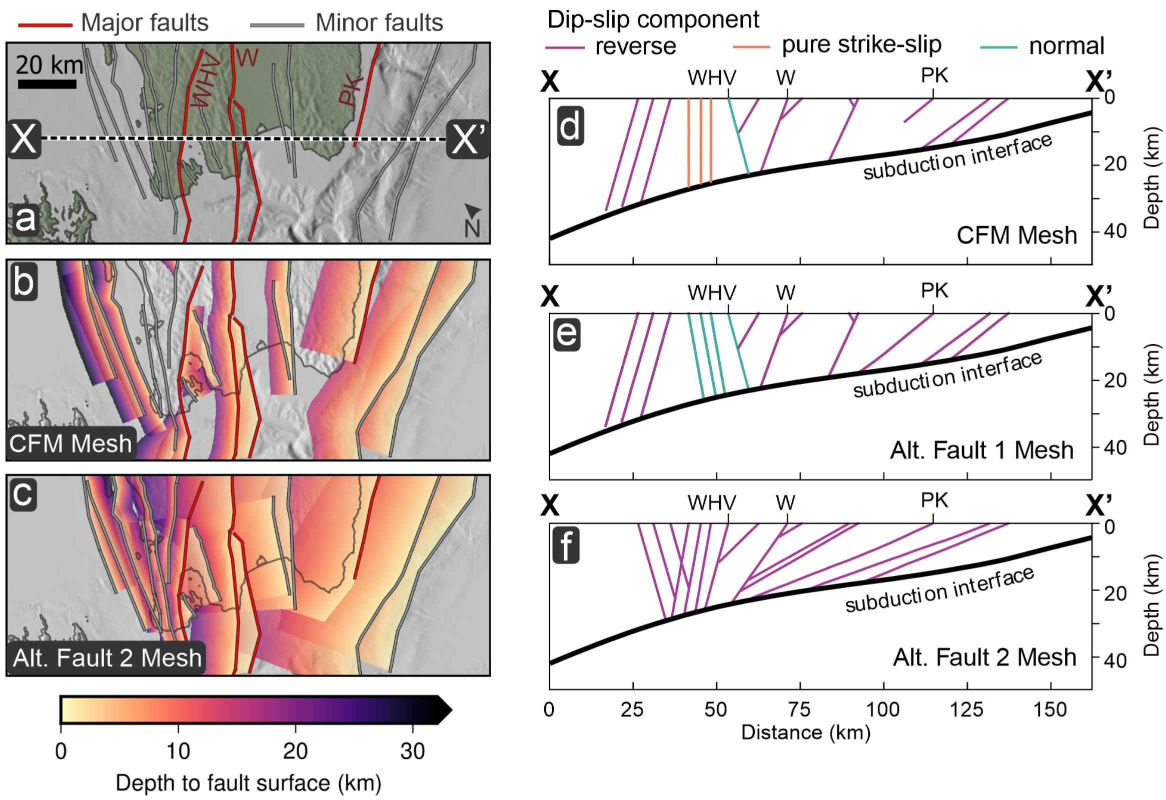

Figure 6: Alternative models of fault geometry for the Greater Wellington Region, after Delano et al. (2024). (a) Map of the coastal part of the Greater Wellington Region. Selected "major" faults are in red, other faults are grey. WHV is the Hutt Valley section of the Wellington Fault (formed of three segments). W is the Wairarapa Fault and PK is the Palliser-Kaiwhata Fault. (b) Map view of fault meshes using the original NZ CFM fault dips and dip directions. (c) Map view of "Alternative Faults 2" meshes, which has fault geometries to represent a plausible suite of fault geometries with generally shallower dips. (d) Cross section through the CFM fault meshes along the line X-X' in (a). (e) Cross section through "Alternative Faults 1" meshes, a suite of geometries that is similar to the NZ CFM, but accounts for a component of normal-sense slip on the predominantly strike-slip Wellington Fault. (f) Cross section through "Alternative Faults 2" meshes.

provements to the workflow could include a wider variety of options to handle fault intersections that involve cross-cutting surfaces at depth.

Listric faults. Our present workflow generates contours by assuming a constant dip for each fault segment, when realistically many (or even most) faults have dips that vary with depth. A possible future expansion of our methodology would be to allow fault dips to vary with depth, as some other workflows allow. Dip-dependent fault geometries could be incorporated by incorporating depth-dip profiles (or similar) for faults of interest at the contour-generation stage. Alternatively, for fault networks like that of Aotearoa New Zealand — for which down-dip variations in fault geometry are only available for a few faults — it may be practical to build meshes for faults with complex geometry manually using Leapfrog or other geological modelling software, and integrate them with the rest of the fault network model as a post-processing stage.

Meshing for other applications. For applications that involve stress transfer between fault elements — examples include boundary-element dynamic earthquake rupture simulations or multi-cycle earthquake simulators like RSQSim — it is often important to align triangle vertices to achieve realistic transfer of stress and to avoid stress singularities. Such alignment of triangle vertices is difficult without meshing multiple fault surfaces simultaneously in dedicated meshing software (for example, Coreform Cubit, Simmetrix SimModeler or Autodesk Fusion360), and to our knowledge has not been achieved for a large fault network (50 or more faults). Our present workflow overcomes this issue for at least one use case (RSQSim) by enforcing a gap (100 m to 2 km) around branch lines where fault meshes would otherwise intersect (see above) to avoid stress singularities. However, for many other use cases this workaround is unlikely to be effective, especially if stress interactions between neighbouring triangles are more sensitive than RSQSim to vertex alignment.

Open-source meshing tools. While the first part of our workflow comprises open-source python tools, the later stages rely on proprietary Leapfrog geological modelling software, including a dedicated bespoke build of Leapfrog to streamline some mesh-cutting operations. Ideally, the whole workflow would use open-source tools. Such an open-source workflow could be practical in future, given the availability of open source tools for mesh generation and cutting like GMsh and mcut. However, we found it easier to use Leapfrog to develop the workflow, and adaptation to rely entirely on open-source software would require significant additional effort.

6 Conclusions

We present a new workflow for the creation of 3D models of complex fault networks, using a mixture of python tools and proprietary geological modelling software. For the case of the Aotearoa New Zealand Community Fault Model (NZ CFM), our workflow reduces the manual labour required to create a model of $\sim$500–800 faults from weeks to days or even hours. The new methodology has already proved useful for local applications in Aotearoa New Zealand earthquake science; our model of faults in central Aotearoa New Zealand has been used to generate synthetic earthquake catalogues using RSQSim, and the alternative models of fault geometry presented in Section 4.2 underpin ongoing efforts to model coseismic coastal deformation hazard in the Greater Wellington Region. Some aspects of our present workflow are limited and there is scope for further development, notably in dealing with fault intersections at depth, depth-dependence of fault dip, and the adoption of more open-source tools in place of proprietary software. Nevertheless, we hope that our new workflow represents a valuable first step towards the efficient creation of 3D models of networks of hundreds of faults.

Acknowledgements

The models in this work were generated using Bentley Software; we thank Bentley Systems Ltd for their provision of Leapfrog software licences and in-kind support of TM, without which the project would not have been possible.

We also gratefully acknowledge Aotearoa New Zealand's Ministry of Business, Innovation and Employment (MBIE) who were the primary funders of this work through: the Resilience to Nature's Challenges Earthquake and Tsunami Theme; Aotearoa New Zealand's National Seismic Hazard Model 2022 Revision Project (contract number 2020-BD101); and the "Ngā Ngāru Wakapuke: Building resilience to future earthquake sequences" and "Te Ao HuriHuri, Te Ao Hou: Our Changing Coast" Endeavour Programmes (contracts RTVU2306 and RTVU2206). We also acknowledge funding from "No Mātou Hapa: It's Our Fault".

Author contributions

AH and TM conceived the project and developed the workflow. AH wrote the python pre-processing tools and TM built a beta version of Seequent's Leapfrog Energy software to automate meshing operations. CP and HS conducted thorough testing of the workflow and built most of the large-scale fault models. AN, BF and RVD organised funding for the project and provided advice on the workflow. CW provided advice on meshing methodology and the development of pre-processing tools. AH wrote the manuscript, with support from all other authors.

Data availability

Python pre-processing tools are available from https://github.com/uc-eqgeo/cfm_leapfrog, with documentation for their use at https://uc-eqgeo.github.io/cfm_leapfrog/. The GitHub repository and a PDF copy of the documentation are also archived on Zenodo: Howell et al. (2025). For information on Leapfrog software, visit https://www.seequent.com/. The meshing steps described here can be accomplished manually in the commercially-available versions of Leapfrog™, but anyone wishing to model more than 100 faults may prefer to contact the authors to discuss use of a beta build that automates several meshing steps.

References

Ando, R. and Kaneko, Y. (2018). Dynamic Rupture Simulation Reproduces Spontaneous Multifault Rupture and Arrest During the 2016 Mw 7.9 Kaikoura Earthquake. *Geophysical Research Letters*, 45(23):12,875–12,883.

Beavan, J., Motagh, M., Fielding, E. J., Donnelly, N., and Collett, D. (2012). Fault slip models of the 2010–2011 Canterbury, New Zealand, earthquakes from geodetic data and observations of postseismic ground deformation. *New Zealand Journal of Geology and Geophysics*, 55(3):207–221. Publisher: Taylor & Francis _eprint: https://doi.org/10.1080/00288306.2012.697472.

Beavan, J., Tregoning, P., Bevis, M., Kato, T., and Meertens, C. (2002). Motion and rigidity of the Pacific Plate and implications for plate boundary deformation. *Journal of Geophysical Research: Solid Earth*, 107(B10):ETG 19–1–ETG 19–15.

Caputo, R., Chatzipetros, A., Pavlides, S., and Sboras, S. (2012). The Greek Database of Seismogenic Sources (GreDaSS): state-of-the-art for northern Greece. *Annals of Geophysics*, 55(5):859–894.

Chan, C.-H., Ma, K.-F., Shyu, J. B. H., Lee, Y.-T., Wang, Y.-J., Gao, J.-C., Yen, Y.-T., and Rau, R.-J. (2020). Probabilistic seismic hazard assessment for Taiwan: TEM PSHA2020. *Earthquake Spectra*, 36(1_suppl):137–159.

Clark, K. J., Nissen, E. K., Howarth, J. D., Hamling, I. J., Mountjoy, J. J., Ries, W. F., Jones, K., Goldstien, S., Cochran, U. A., Villamor, P., Hreinsdóttir, S., Litchfield, N. J., Mueller, C., Berryman, K. R., and Strong, D. T. (2017). Highly variable coastal deformation in the 2016 Mw7.8 Kaikōura earthquake reflects rupture complexity along a transpressional plate boundary. *Earth and Planetary Science Letters*, 474:334–344.

Darby, D. J. and Beanland, S. (1992). Possible source models for the 1855 Wairarapa Earthquake, New Zealand. *Journal of Geophysical Research: Solid Earth*, 97(B9):12375–12389. _eprint: https://onlinelibrary.wiley.com/doi/pdf/10.1029/92JB00567.

Delano, J., Howell, A., Clark, K., Stahl, T., Rollins, C., Seebeck, H., and McGrath, J. (2024). A probabilistic model for coseismic vertical displacement hazard in coastal settings. *Geosphere*, submitted.

Delano, J. E., Howell, A., Clark, K. J., and Stahl, T. A. (2023). Upper Plate Faults May Contribute to the Paleoseismic Subsidence Record Along the Central Hikurangi Subduction Zone, Aotearoa New Zealand. *Geochemistry, Geophysics, Geosystems*, 24(10):e2023GC011060. _eprint: https://onlinelibrary.wiley.com/doi/pdf/10.1029/2023GC011060.

Delano, J. E., Howell, A., Stahl, T. A., and Clark, K. (2022). 3D Coseismic Surface Displacements From Historical Aerial Photographs of the 1987 Edgecumbe Earthquake, New Zealand. *Journal of Geophysical Research: Solid Earth*, 127(11):e2022JB024059. _eprint: https://onlinelibrary.wiley.com/doi/pdf/10.1029/2022JB024059.

Delogkos, E., Howell, A., Seebeck, H., Shaw, B. E., Nicol, A., Mika Liao, Y.-W., and Walsh, J. J. (2023). Impact of Variable Fault Geometries and Slip Rates on Earthquake Catalogs From Physics-Based Simulations of a Normal Fault. *Journal of Geophysical Research: Solid Earth*, 128(11):e2023JB026746. _eprint: https://onlinelibrary.wiley.com/doi/pdf/10.1029/2023JB026746.

Elliott, J. R., Nissen, E. K., England, P. C., Jackson, J. A., Lamb, S., Li, Z., Oehlers, M., and Parsons, B. (2012).

Slip in the 2010–2011 Canterbury earthquakes, New Zealand. *Journal of Geophysical Research: Solid Earth*, 117(B3).

Ellis, S., Bannister, S., Van Dissen, R., Eberhart-Phillips, D., Boulton, C., Reyners, M., Funnell, R., Mortimer, N., Upton, P., Rollins, C., and Seebeck, H. (2024). New Zealand Fault-Rupture Depth Model v.1.0: A Provisional Estimate of the Maximum Depth of Seismic Rupture on New Zealand's Active Faults. *Bulletin of the Seismological Society of America*, 114(1):78–94.

Ellis, S. M., Bannister, S., Van Dissen, R. J., Eberhart-Phillips, D., Boulton, C. J., Reyners, M., Funnell, R. H., Mortimer, N., and Upton, P. (2021). *New Zealand Fault-rupture Depth Model V1. 0: A Provisional Estimate of the Maximum Depth of Seismic Rupture on New Zealand's Active Faults*. GNS Science Te Pū Ao.

Faure Walker, J. P., Visini, F., Roberts, G., Galasso, C., McCaffrey, K., and Mildon, Z. (2018). Variable Fault Geometry Suggests Detailed Fault-Slip-Rate Profiles and Geometries Are Needed for Fault-Based Probabilistic Seismic Hazard Assessment (PSHA). *Bulletin of the Seismological Society of America*, 109(1):110–123.

Field, E. H., Arrowsmith, R. J., Biasi, G. P., Bird, P., Dawson, T. E., Felzer, K. R., Jackson, D. D., Johnson, K. M., Jordan, T. H., Madden, C., Michael, A. J., Milner, K. R., Page, M. T., Parsons, T., Powers, P. M., Shaw, B. E., Thatcher, W. R., Weldon, R. J., and Zeng, Y. (2014). Uniform California Earthquake Rupture Forecast, Version 3 (UCERF3)—The Time-Independent Model. *Bulletin of the Seismological Society of America*, 104(3):1122–1180.

Fujiwara, H., Kawai, S., Aoi, S., Morikawa, N., Senna, S., Kudo, N., Ooi, M., Hao, K., Wakamatsu, K., Ishikawa, Y., and others (2009). Technical reports on national seismic hazard maps for Japan. *Technical Note of the National Research Institute for Earth Science and Disaster Prevention*, 336.

Gerstenberger, M. C., Bora, S., Bradley, B. A., DiCaprio, C., Kaiser, A., Manea, E. F., Nicol, A., Rollins, C., Stirling, M. W., Thingbaijam, K. K. S., Van Dissen, R. J., Abbott, E. R., Atkinson, G. M., Chamberlain, C., Christophersen, A., Clark, K., Coffey, G. L., de la Torre, C. A., Ellis, S. M., Fraser, J., Graham, K., Griffin, J., Hamling, I. J., Hill, M. P., Howell, A., Hulsey, A., Hutchinson, J., Iturrieta, P., Johnson, K. M., Jurgens, V. O., Kirkman, R., Langridge, R. M., Lee, R. L., Litchfield, N. J., Maurer, J., Milner, K. R., Rastin, S., Rattenbury, M. S., Rhoades, D. A., Ristau, J., Schorlemmer, D., Seebeck, H., Shaw, B. E., Stafford, P. J., Stolte, A. C., Townend, J., Villamor, P., Wallace, L. M., Weatherill, G., Williams, C. A., and Wotherspoon, L. M. (2024a). The 2022 Aotearoa New Zealand National Seismic Hazard Model: Process, Overview, and Results. *Bulletin of the Seismological Society of America*.

Gerstenberger, M. C., Marzocchi, W., Allen, T., Pagani, M., Adams, J., Danciu, L., Field, E. H., Fujiwara, H., Luco, N., Ma, K.-F., Meletti, C., and Petersen, M. D. (2020). Probabilistic Seismic Hazard Analysis at Regional and National Scales: State of the Art and Future Challenges. *Reviews of Geophysics*, 58(2):e2019RG000653. _eprint: https://onlinelibrary.wiley.com/doi/pdf/10.1029/2019RG000653.

Gerstenberger, M. C., Van Dissen, R., Rollins, C., DiCaprio, C., Thingbaijim, K. K. S., Bora, S., Chamberlain, C., Christophersen, A., Coffey, G. L., Ellis, S. M., Iturrieta, P., Johnson, K. M., Litchfield, N. J., Nicol, A., Milner, K. R., Rastin, S. J., Rhoades, D., Seebeck, H., Shaw, B. E., Stirling, M. W., Wallace, L., Allen, T. I., Bradley, B. A., Charlton, D., Clark, K. J., Fraser, J., Griffin, J., Hamling, I. J., Howell, A., Hudson-Doyle, E., Hulsey, A., Jurgens, V. O., Kaiser, A. E., Kirkman, R., Langridge, R. M., Maurer, J., Rattenbury, M. S., Ristau, J., Schorlemmer, D., Townend, J., Villamor, P., and Williams, C. (2024b). The Seismicity Rate Model for the 2022 Aotearoa New Zealand National Seismic Hazard Model. *Bulletin of the Seismological Society of America*.

Hagberg, A., Swart, P., and S Chult, D. (2008). Exploring network structure, dynamics, and function using networkx.

Hamling, I. J., Hreinsdóttir, S., Clark, K., Elliott, J., Liang, C., Fielding, E., Litchfield, N., Villamor, P., Wallace, L., Wright, T. J., D'Anastasio, E., Bannister, S., Burbidge, D., Denys, P., Gentle, P., Howarth, J., Mueller, C., Palmer, N., Pearson, C., Power, W., Barnes, P., Barrell, D. J. A., Van Dissen, R. J., Langridge, R., Little, T., Nicol, A., Pettinga, J., Rowland, J., and Stirling, M. (2017). Complex multifault rupture during the 2016 Mw 7.8 Kaikōura earthquake, New Zealand. *Science*, 356(6334):eaam7194.

Howarth, J. D., Barth, N. C., Fitzsimons, S. J., Richards-Dinger, K., Clark, K. J., Biasi, G. P., Cochran, U. A., Langridge, R. M., Berryman, K. R., and Sutherland, R. (2021). Spatiotemporal clustering of great earthquakes on a transform fault controlled by geometry. *Nature Geoscience*, 14(5):314–320. Publisher: Nature Publishing Group.

Howell, A., McLennan, T., Penney, C., Nicol, A., Seebeck, H., Van Dissen, R. J., Williams, C. A., and Fry, B. (2025). A semi-automated method for constructing three-dimensional models of complex fault networks. *Tektonika*, in review.

Hughes, L., Power, W., Lane, E. M., Savage, M. K., Arnold, R., Howell, A., Shaw, B., Fry, B., and Nicol, A. (2023). A Novel Method to Determine Probabilistic Tsunami Hazard Using a Physics-Based Synthetic Earthquake Catalog: A New Zealand Case Study. *Journal of Geophysical Research: Solid Earth*, 128(12):e2023JB027207. _eprint: https://onlinelibrary.wiley.com/doi/pdf/10.1029/2023JB027207.

Hughes, M. W., Quigley, M. C., Van Ballegooy, S., Deam, B. L., Bradley, B. A., Hart, D. E., and Measures, R. (2015). The sinking city: Earthquakes increase flood hazard in Christchurch, New Zealand. *GSA Today*, 25(3):4–10. Publisher: Geological Society of America.

Hull, A. G. (1990). Tectonics of the 1931 Hawke's Bay earthquake. *New Zealand Journal of Geology and Geophysics*, 33(2):309–320. Publisher: Taylor & Francis _eprint: https://doi.org/10.1080/00288306.1990.10425689.

Johnson, K. M., Wallace, L. M., Maurer, J., Hamling, I., Williams, C., Rollins, C., Gerstenberger, M., and Van Dissen, R. (2024). Inverting Geodetic Strain Rates for Slip Deficit Rate in Complex Deforming Zones: An Application to the New Zealand Plate Boundary. *Journal of Geophysical Research: Solid Earth*, 129(3):e2023JB027565. _eprint: https://onlinelibrary.wiley.com/doi/pdf/10.1029/2023JB027565.

Litchfield, N. J., Van Dissen, R. J., Sutherland, R., Barnes, P. M., Cox, S. C., Norris, R., Beavan, R. J., Langridge, R., Villamor, P., Berryman, K., Stirling, M., Nicol, A., Nodder, S., Lamarche, G., Barrell, D. J. A., Pettinga, J. R., Little, T., Pondard, N., Mountjoy, J. J., and Clark, K. (2014). A model of active faulting in New Zealand. *New Zealand Journal of Geology and Geophysics*, 57(1):32–56. Publisher: Taylor & Francis _eprint: https://doi.org/10.1080/00288306.2013.854256.

Liu, C., Lay, T., Brodsky, E. E., Dascher-Cousineau, K., and Xiong, X. (2019). Coseismic Rupture Process of the Large 2019 Ridgecrest Earthquakes From Joint Inversion of Geodetic and Seismological Observations. *Geophysical Research Letters*, 46(21):11820–11829. _eprint: https://onlinelibrary.wiley.com/doi/pdf/10.1029/2019GL084949.

Lozos, J. C. (2016). A case for historic joint rupture of the San Andreas and San Jacinto faults. *Science Advances*, 2(3):e1500621. Publisher: American Association for the Advancement of Science.

Mildon, Z. K., Roberts, G. P., Walker, J. P. F., and Toda, S. (2019). Coulomb pre-stress and fault bends are ignored yet vital factors for earthquake triggering and hazard. *Nature Communications*, 10(1):1–9.

Mildon, Z. K., Toda, S., Faure Walker, J. P., and Roberts, G. P. (2016). Evaluating models of Coulomb stress transfer: Is variable fault geometry important? *Geophysical Research Letters*, 43(24):12,407–12,414. _eprint: https://onlinelibrary.wiley.com/doi/pdf/10.1002/2016GL071128.

Naish, T., Levy, R., Hamling, I., Hreinsdóttir, S., Kumar, P., Garner, G. G., Kopp, R. E., Golledge, N., Bell, R., Paulik, R., Lawrence, J., Denys, P., Gillies, T., Bengtson, S., Howell, A., Clark, K., King, D., Litchfield, N., and Newnham, R. (2024). The Significance of Interseismic Vertical Land Movement at Convergent Plate Boundaries in Probabilistic Sea-Level Projections for AR6 Scenarios: The New Zealand Case. *Earth's Future*, 12(6):e2023EF004165. _eprint: https://onlinelibrary.wiley.com/doi/pdf/10.1029/2023EF004165.

Oglesby, D. D. and Mai, P. M. (2012). Fault geometry, rupture dynamics and ground motion from potential earthquakes on the North Anatolian Fault under the Sea of Marmara. *Geophysical Journal International*, 188(3):1071–1087.

Okada, Y. (1985). Surface deformation due to shear and tensile faults in a half-space. *Bulletin of the seismological society of America*, 75(4):1135–1154. Publisher: The Seismological Society of America.

Pagani, M., Garcia-Pelaez, J., Gee, R., Johnson, K., Poggi, V., Silva, V., Simionato, M., Styron, R., Viganò, D., Danciu, L., Monelli, D., and Weatherill, G. (2020). The 2018 version of the Global Earthquake Model:

Hazard component. *Earthquake Spectra*, 36(1_suppl):226–251.

Plesch, A., Marshall, S. T., Nicholson, C., Shaw, J. H., Maechling, P. J., and Su, M. (2020). The Community Fault Model version 5.3 and new web-based tools. In *SCEC Annual Meeting, Poster*, volume 184.

Plesch, A., Shaw, J. H., Benson, C., Bryant, W. A., Carena, S., Cooke, M., Dolan, J., Fuis, G., Gath, E., Grant, L., Hauksson, E., Jordan, T., Kamerling, M., Legg, M., Lindvall, S., Magistrale, H., Nicholson, C., Niemi, N., Oskin, M., Perry, S., Planansky, G., Rockwell, T., Shearer, P., Sorlien, C., Süss, M. P., Suppe, J., Treiman, J., and Yeats, R. (2007). Community Fault Model (CFM) for Southern California. *Bulletin of the Seismological Society of America*, 97(6):1793–1802.

Richards-Dinger, K. and Dieterich, J. H. (2012). RSQSim Earthquake Simulator. *Seismological Research Letters*, 83(6):983–990.

Robinson, R. (2004). Potential earthquake triggering in a complex fault network: the northern South Island, New Zealand. *Geophysical Journal International*, 159(2):734–748.

Robinson, R., Van Dissen, R., and Litchfield, N. (2011). Using synthetic seismicity to evaluate seismic hazard in the Wellington region, New Zealand. *Geophysical Journal International*, 187(1):510–528. Publisher: Oxford Academic.

Satake, K., Ishibe, T., Murotani, S., Mulia, I. E., and Gusman, A. R. (2022). Effects of uncertainty in fault parameters on deterministic tsunami hazard assessment: examples for active faults along the eastern margin of the Sea of Japan. *Earth, Planets and Space*, 74(1):36.

Seebeck, H., Van Dissen, R., Litchfield, N., Barnes, P., Nicol, A., Langridge, R., Barrell, D., Villamor, P., Ellis, S., Rattenbury, M., and others (2022). New Zealand Community Fault Model–version 1.0. Publisher: GNS Science.

Seebeck, H., Van Dissen, R. J., Litchfield, N., Barnes, P. M., Nicol, A., Langridge, R., Barrell, D. J. A., Villamor, P., Ellis, S., Rattenbury, M., Bannister, S., Gerstenberger, M., Ghisetti, F., Sutherland, R., Hirschberg, H., Fraser, J., Nodder, S. D., Stirling, M., Humphrey, J., Bland, K. J., Howell, A., Mountjoy, J., Moon, V., Stahl, T., Spinardi, F., Townsend, D., Clark, K., Hamling, I., Cox, S., de Lange, W., Wopereis, P., Johnston, M., Morgenstern, R., Coffey, G., Eccles, J. D., Little, T., Fry, B., Griffin, J., Townend, J., Mortimer, N., Alcaraz, S., Massiot, C., Rowland, J. V., Muirhead, J., Upton, P., and Lee, J. (2023). The New Zealand Community Fault Model – version 1.0: an improved geological foundation for seismic hazard modelling. *New Zealand Journal of Geology and Geophysics*, 0(0):1–21. Publisher: Taylor & Francis _eprint: https://doi.org/10.1080/00288306.2023.2181362.

Shaw, B. E., Fry, B., Nicol, A., Howell, A., and Gerstenberger, M. (2022). An Earthquake Simulator for New Zealand. *Bulletin of the Seismological Society of America*, 112(2):763–778.

Stirling, M., McVerry, G., Gerstenberger, M., Litchfield, N., Van Dissen, R., Berryman, K., Barnes, P., Wallace, L., Villamor, P., Langridge, R., Lamarche, G., Nodder, S., Reyners, M., Bradley, B., Rhoades, D., Smith, W., Nicol, A., Pettinga, J., Clark, K., and Jacobs, K. (2012). National Seismic Hazard Model for New Zealand: 2010 Update. *Bulletin of the Seismological Society of America*, 102(4):1514–1542.

Ulrich, T., Gabriel, A.-A., Ampuero, J.-P., and Xu, W. (2019a). Dynamic viability of the 2016 Mw 7.8 Kaikōura earthquake cascade on weak crustal faults. *Nature Communications*, 10(1):1213.

Ulrich, T., Vater, S., Madden, E. H., Behrens, J., van Dinther, Y., van Zelst, I., Fielding, E. J., Liang, C., and Gabriel, A.-A. (2019b). Coupled, Physics-Based Modeling Reveals Earthquake Displacements are Critical to the 2018 Palu, Sulawesi Tsunami. *Pure and Applied Geophysics*, 176(10):4069–4109.

Van Dissen, R. J., Johnson, K. M., Seebeck, H., Wallace, L. M., Rollins, C., Maurer, J., Gerstenberger, M. C., Williams, C. A., Hamling, I. J., Howell, A., and DiCaprio, C. J. (2024). Upper Plate and Subduction Interface Deformation Models in the 2022 Revision of the Aotearoa New Zealand National Seismic Hazard Model. *Bulletin of the Seismological Society of America*, 114(1):37–56.

Villamor, P., Litchfield, N., Barrell, D., Van Dissen, R. J., Hornblow, S., Quigley, M., Levick, S., Ries, W., Duffy, B., Begg, J., Townsend, D., Stahl, T., Bilderback, E., Noble, D., Furlong, K., and Grant, H. (2012). Map of the 2010 Greendale Fault surface rupture, Canterbury, New Zealand: application to land use planning. *New Zealand Journal of Geology and Geophysics*, 55(3):223–230.

Wesnousky, S. G. (2008). Displacement and Geometrical Characteristics of Earthquake Surface Ruptures: Issues and Implications for Seismic-Hazard Analysis and the Process of Earthquake Rupture. *Bulletin of the Seismological Society of America*, 98(4):1609–1632.

Williams, C. A., Eberhart-Phillips, D., Bannister, S., Barker, D. H. N., Henrys, S., Reyners, M., and Sutherland, R. (2013). Revised Interface Geometry for the Hikurangi Subduction Zone, New Zealand. *Seismological Research Letters*, 84(6):1066–1073. Publisher: GeoScienceWorld.

Williams, J. N., Wedmore, L. N. J., Scholz, C. A., Kolawole, F., Wright, L. J. M., Shillington, D. J., Fagereng, A., Biggs, J., Mdala, H., Dulanya, Z., Mphepo, F., Chindandali, P. R. N., and Werner, M. J. (2022). The Malawi Active Fault Database: An Onshore-Offshore Database for Regional Assessment of Seismic Hazard and Tectonic Evolution. *Geochemistry, Geophysics, Geosystems*, 23(5):e2022GC010425. _eprint: https://onlinelibrary.wiley.com/doi/pdf/10.1029/2022GC010425.